Highly Improved Rate Capability for a Lithium-Ion Battery Nano-$Li_4Ti_5O_{12}$ Negative Electrode via Carbon-Coated Mesoporous Uniform Pores with a Simple Self-Assembly Method

Eunae Kang, Yoon Seok Jung, Gi-Heon Kim, Jinyoung Chun, Ulrich Wiesner, Anne C. Dillon, Jin Kon Kim,* and Jinwoo Lee**

A mesostructured spinel $Li_4Ti_5O_{12}$ (LTO)-carbon nanocomposite (denoted as Meso-LTO-C) with large (>15 nm) and uniform pores is simply synthesized via block copolymer self-assembly. Exceptionally high rate capability is then demonstrated for Li-ion battery (LIB) negative electrodes. Polyisoprene-*block*-poly(ethylene oxide) (PI-*b*-PEO) with a sp^2-hybridized carbon-containing hydrophobic block is employed as a structure-directing agent. Then the assembled composite material is crystallized at 700 °C enabling conversion to the spinel LTO structure without loss of structural integrity. Part of the PI is converted to a conductive carbon that coats the pores of the Meso-LTO-C. The in situ pyrolyzed carbon not only maintains the porous mesostructure as the LTO is crystallized, but also improves the electronic conductivity. A Meso-LTO-C/Li cell then cycles stably at 10 C-rate, corresponding to only 6 min for complete charge and discharge, with a reversible capacity of 115 mA h g^{-1} with 90% capacity retention after 500 cycles. In sharp contrast, a Bulk-LTO/Li cell exhibits only 69 mA h g^{-1} at 10 C-rate. Electrochemical impedance spectroscopy (EIS) with symmetric LTO/LTO cells prepared from Bulk-LTO and Meso-LTO-C cycled in different potential ranges reveals the factors contributing to the vast difference between the rate-capabilities. The carbon-coated mesoporous structure enables highly improved electronic conductivity and significantly reduced charge transfer resistance, and a much smaller overall resistance is observed compared to Bulk-LTO. Also, the solid electrolyte interphase (SEI)-free surface due to the limited voltage window (>1 V versus Li/Li^+) contributes to dramatically reduced resistance.

1. Introduction

Recently, considerable efforts have been made to develop high performance Li-ion batteries (LIBs) for new applications including plug-in hybrid electric vehicles (PHEVs) and electric vehicles (EVs).[1] Spinel $Li_4Ti_5O_{12}$ (LTO) is an alternative negative electrode material for LIBs due to several important advantages in spite of lower theoretical capacity ($Li_4Ti_5O_{12} + 3Li^+ + 3e^- \rightarrow Li_7Ti_5O_{12}$, 175 mA h g^{-1}) than already commercialized graphite (372 mA h g^{-1}). First, Ti is an abundant element allowing it to be a cost-effective material.[2] Furthermore, LTO exhibits a Li^+ insertion/extraction potential of ~1.55 V (vs. Li/Li^+). This enables LTO electrodes not to suffer from many critical problems caused by undesirable electrolyte decomposition that occurs at reductive potentials under ~1 V (vs. Li/Li^+).[1a,3] The side reactions not only lead to the formation of a solid electrolyte interphase (SEI) film and gas evolution but also result in low coulombic efficiency especially in the first formation cycle due to a significant loss of Li^+.[4] It is also known that the

E. Kang, J. Chun, Prof. Dr. J. K. Kim, Prof. Dr. J. Lee
Department of Chemical Engineering
Pohang University of Science and Technology
San 31, Hyo-ja dong, Pohang, 790-784, Korea
E-mail: jkkim@postech.ac.kr; jinwoo03@postech.ac.kr
Prof. Dr. J. Lee
School of Environmental Science and Engineering
Pohang University of Science and Technology
San 31, Hyo-ja dong, Pohang, 790-784, Korea
Dr. Y. S. Jung, Dr. G.-H. Kim, Dr. A. C. Dillon
National Renewable Energy Laboratory
Golden, CO80401, USA
Email: anne.dillon@nrel.gov
Prof. Dr. Y. S. Jung
Interdisciplinary School of Green Energy
Ulsan National Institute of Science and Technology (UNIST)
Ulsan 689-798, Korea
Prof. Dr. U. Wiesner
Department of Materials Science and Engineering
Cornell University, Ithaca, NY 14853, USA

DOI: 10.1002/adfm.201101123

stability and or lack of the SEI plays a key role in the negative electrode durability, safety, rate capability, etc.[4c,4h,5] Efforts have been focused on developing high-capacity nanostructured negative electrode materials (e.g., nanowires, nanoparticles, etc.) that operate at low potential (<1 V vs. Li/Li^+) due to improved capacity durability, rate capability, etc.[6] However, it is unlikely that these nanostructured electrode materials will be used for practical applications because of the severe side reactions at low operating potential and extremely large surface areas. Specifically, the high operating potential of LTO ensures that Li plating does not occur,[2d,7] which can lead to internal short circuits, a serious safety concern especially in large format LIBs.[8] LTO is also known to show exceptional durability because of negligible volume expansion/contraction, <1%[2c,9] while graphite experiences ~13% volume change during full charge–discharge,[10] and intrinsically high Li-ion mobility.[11]

The major drawback of LTO is that it is electrically insulating ($<10^{-13}$ S cm^{-1}).[12] Several approaches to improve the electronic conductivity[13–17] include carbon coating via chemical vapor deposition (CVD),[13] nanocomposite formation with multi-walled carbon nanotubes,[14] metal doping,[15,16] and nitridation on the surface.[17] Another approach to overcome low electrical conductivity is to employ nanostructures, as the reduced dimension significantly shortens the electronic path. In addition, the nanostructures also enable facile transport of the electrolyte to the surfaces of electrochemically active materials, resulting in rapid charge transfer reactions due to the high electrode-electrolyte interface area, and short Li^+ diffusion paths.[18] Thus there have been many research efforts to develop nano-sized materials for high rate capability electrodes.[1b,1d,1g,2d,6] However, the nano-sized materials suffer from low packing density,[19] resulting in low volumetric density. Furthermore, it is also possible that the nanoparticles may be released from the electrode surface, cross the separator and cause an internal short circuit, as the separator used in commercial battery systems has approximately 1 μm pores.[18b]

To overcome these problems associated with the nano-sized materials, it is desirable to create a conductive and porous matrix for micrometer-sized particles that provides good particle-particle contact. Namely, mesostructured materials with large open pores, which were first synthesized through a self-assembly method for nanocatalysis,[20] are ideal candidates. For the mesostructured materials, the particles remain micrometer-sized but contain pores of nanometer dimension separated by nanometer-thick walls.[21] Micrometer-sized mesostructured particles containing nanostructures can also be fabricated into composite electrodes, leading to a similar packing density. The well defined and interconnected nanostructure then ensures a high electrolyte/electrode interfacial area and short Li-ion diffusion length. The uniform and well-interconnected pores minimize wasted volume mainly due to larger pores and inactive pores between nanoparticles.[2e]

Because of the advantages described above, various mesostructured materials have been synthesized and used as both negative and positive electrodes for LIBs. For example, Bruce and coworkers group synthesized mesoporous $LiMn_2O_4$, TiO_2 (anatase), and $LiCoO_2$ by using mesostructured silica as a hard template.[22] Because heat-treatment at high temperature cannot be conducted for soft-templates[23] such as block copolymers, the hard template method is typically employed to make mesoporous electrode materials. However, the hard template method requires a long synthesis time (typically more than 7 days) and tedious multi-steps to acquire the final products. Also, a toxic hydrofluoric acid (HF) is often used to remove silicate frameworks. Furthermore, Li sources in the precursors can react with the silica hard template.

Recently, researchers have developed hierarchically structured LTO (micrometer-size (~0.5–2 μm)) secondary particles composed of nanometer-size (<10 nm) via a hydrothermal method[19] and three-dimensionally ordered macroporous (3DOM) using poly(methyl methacrylate) colloidal crystal templates for LIBs.[3b] To the best of our knowledge, however, there is no report on the synthesis of mesostructured LTO with uniform and large pores via either soft or hard template method. This is because LTO is typically synthesized at high-temperature (>700 °C),[24] not feasible to fabricate mesostructured LTO using a soft-template method. Although soft-templated mesostructured materials lose their ordered structure at temperature higher than 500 °C,[23] a simple alternative approach called CASH (combined assembly of soft and hard chemistries) could be employed to make thermally stable metal oxides.[25] Laboratory-made amphiphilic block copolymer, such as polyisoprene-*block*-poly(ethylene oxide) (PI-*b*-PEO), was used as a structure directing agent for the assembly with metal oxide sols. The in situ generated carbon acted as a rigid support for the mesostructured oxide walls, preventing collapse during heat-treatment at high temperature (>700 °C).

Herein, for the first time, we report on the synthesis of a mesostructured LTO-carbon nanocomposite (Meso-LTO-C) with large (>15 nm) and uniform pores for a high-performance LIB negative electrode via a block copolymer assembly by employing PI-*b*-PEO. Even though the as-synthesized mesostructured LTO is synthesized through a simple self-assembly method, the as-synthesized materials is crystallized at 700 °C and conductive carbon is coated on the pore walls of mesoporous LTO. The resulting Meso-LTO-C composite has a capacity of 115 mA h g^{-1} at 10 C-rate with exceptionally good cycling performance, 90% of capacity retention after 500 cycles (1.6 A g^{-1}, 1 C-rate = 160 mA h g^{-1}). The effects of the electrode-electrolyte interface or SEI on the kinetics are also investigated in detail with electrochemical impedance spectroscopy (EIS) analysis.

2. Results and Discussion

2.1. Synthesis of Meso-LTO-C.

Synthesis was achieved by the self-assembly of PI-*b*-PEO with titanium tetraisopropoxide, lithium ethoxide, and oxalic acid, which selectively swell the hydrophilic block (PEO). During high-temperature heat-treatment at 700 °C for the formation of the $Li_4Ti_5O_{12}$ spinel phase, most of the block copolymer is burnt off, and part of PI is converted to carbon, maintaining the mesostructures (**Scheme 1**). The resulting structure allows the electrolyte to be highly accessible to the active material and maintains a short path length for Li-ions and electrons. Small angle X-ray scattering (SAXS) patterns of as-synthesized LTO and Meso-LTO-C are shown in **Figure 1**a. For the as-synthesized LTO, one single intense peak is observed at

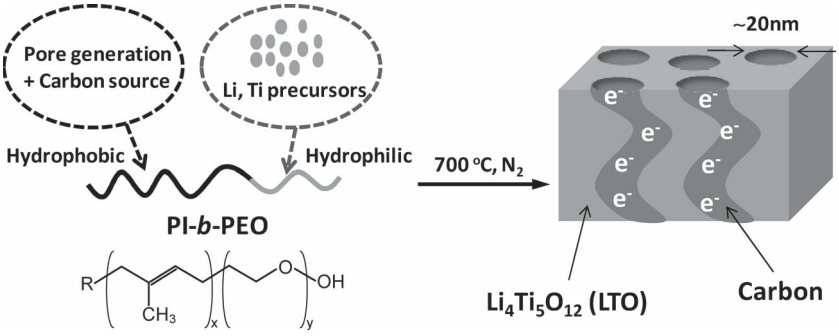

Scheme 1. Schematic representation of the synthesis of Meso-LTO-C.

q = 0.21 nm^{-1} (q denotes the scattering vector), corresponding to a d-spacing of 29.9 nm. One single intense peak represents typical wormhole-like structures or short-range ordered hexagonal structures.[26] After heat-treatment at 700 °C, Meso-LTO-C also shows one single peak that corresponds to a d-spacing of 19.3 nm, indicating that the mesostructure is preserved and shrinkage occurs upon removal of organic molecules. Raman spectroscopy of Meso-LTO-C is shown in Figure 1b. The presence of in situ formed carbon (Figure S1) from the PI block is confirmed by two bands around 1590 cm^{-1} and 1380 cm^{-1} from graphitic carbon (G-band) and disordered carbon (D-band), respectively.[27] The in situ formed carbon not only helps maintain the mesostructure during the heat treatment required to form LTO, but also enables a superior electronic network in the Meso-LTO-C. The presence of carbon is also corroborated using thermogravimetric analysis (TGA) (Figure 1c). About 8.5% weight loss is observed around 400 °C. The wide-angle X-ray diffraction (XRD) pattern of Meso-LTO-C (Figure 1d) shows that the peaks are well indexed to those of $Li_4Ti_5O_{12}$ (Fd3m, JCDPS No. 49-0207). The calculated crystallite size of LTO using the Debye–Scherrer equation[28] and the XRD pattern is 9.5 nm, confirming that the wall of Meso-LTO-C is composed of nanocrytalline LTO, providing a short Li-ion diffusion path.

Field emission scanning electron microscopy (FESEM) images are presented in **Figure 2**. At a low magnification (Figure 2a), it is apparent that the mesopores are well-developed and encompass entire particles. At a higher magnification (Figure 2b), the mesopores are organized in a short-range ordered channel or wormhole-like structure similar to HMS (hexagonal mesoporous silica).[26b] The pore size is around ~20 nm. The wormhole-like structure is believed to be three-dimensionally interconnected, which is favorable for easy access of electrolyte inside the pores.[26,29] The transmission electron microscopy (TEM) image of Meso-LTO-C (Figure 2c)

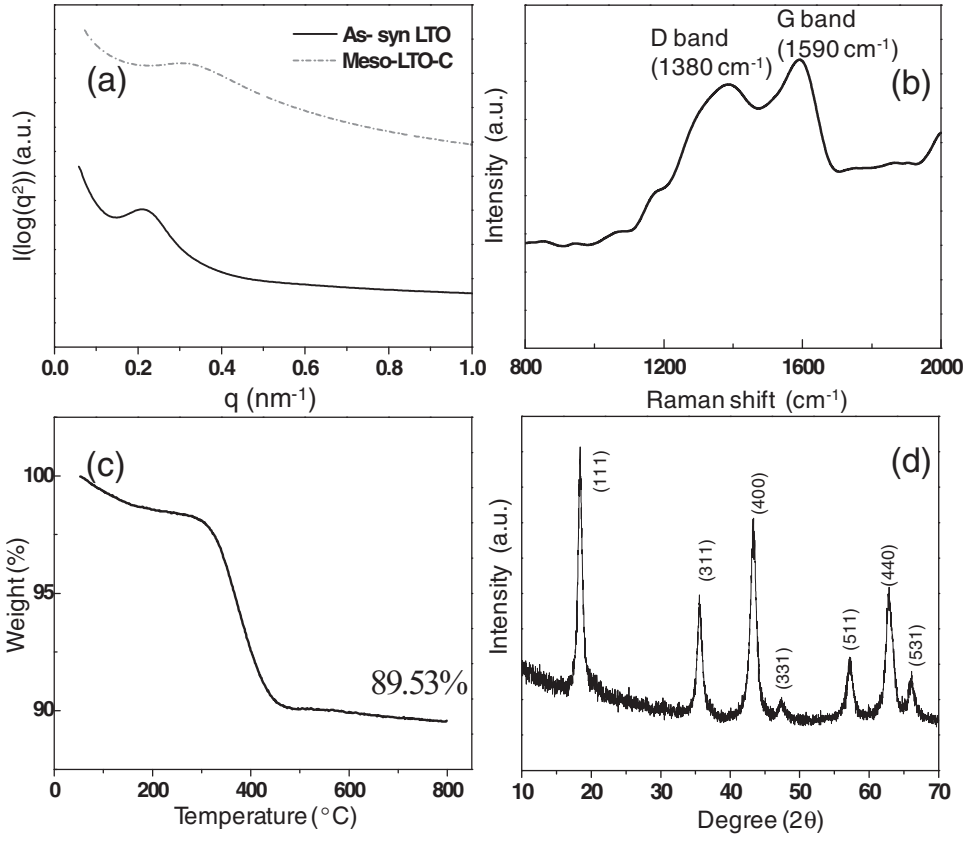

Figure 1. a) SAXS traces of as-synthesized $Li_4Ti_5O_{12}$ and Meso-LTO-C. b) Raman spectrum of Meso-LTO-C. c) TGA profile of Meso-LTO-C. d) Wide-angle powder XRD pattern of Meso-LTO-C.

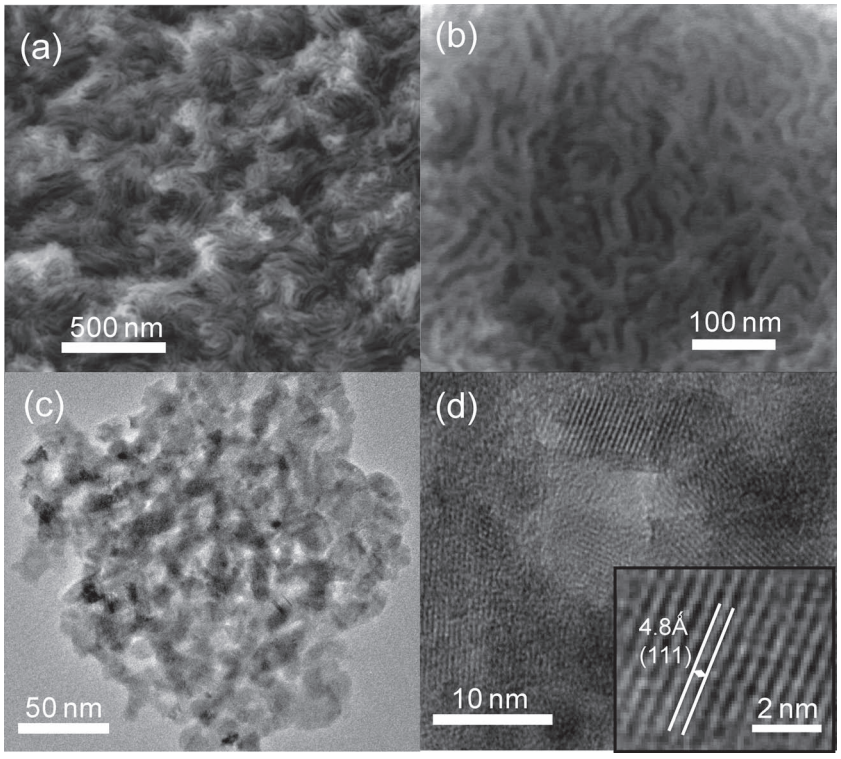

Figure 2. SEM images of Meso-LTO-C at low (a) and higher magnification (b). c) TEM and d) HRTEM image of Meso-LTO-C showing wormhole-like pores.

corroborates the FESEM results, as the wormhole-like pores are again observed to surround entire particles completely. High-resolution TEM (HRTEM) of Meso-LTO-C (Figure 2d) reveals that the walls are composed of nanocrystallites connected to each other. The nanocrystals are randomly oriented and overlap each other within the pore walls. The lattice fringe is clearly observed in the HRTEM image (Figure 2d, inset). The average *d*-spacing is 4.8 Å, which is consistent with the d_{111}-spacing of $Li_4Ti_5O_{12}$ (Fd3m, JCDPS No. 49-0207). This HRTEM image therefore also confirms that the wall is composed of LTO nanocrystallites. Furthermore, electron energy loss spectroscopy (EELS) analysis for Meso-LTO-C (**Figure 3**) shows uniform distribution of Li, Ti, and O all over the structured materials, which suggests that the mesostructure wall is composed of LTO, consistent with the HRTEM image.

The porosity of Meso-LTO-C was studied by nitrogen adsorption-desorption isotherms using a Micromeritics Tristar at 77 K. **Figure 4**a shows a nitrogen isotherm curve of Meso-LTO-C. The isotherm exhibits type IV curves according to the BDDT (Brunauer, Deming, Deming, and Teller) classification, with sharp capillary condensation at p/p_0 of ~0.9, suggesting that large and uniform pores are well-developed. The H1 type hysteresis of the isotherm suggests cylindrical pore geometry.[30] Pore size was calculated to be 20.4 nm based on the Barrett–Joyner–Halenda (BJH) method (Figure 4b). Again these large pores allow easy access of the electrolyte to the active material, which cannot be achieved with commercial block copolymers (Pluronic series) employed typically to make mesoporous metal oxides.[31] The pore volume and surface area are 0.148 $cm^3\ g^{-1}$ and 68.7 $m^2\ g^{-1}$, respectively.

2.2. Electrochemical Characteristics of Meso-LTO-C.

Most importantly, we performed electrochemical characterization for Meso-LTO-C as a negative electrode for LIBs. As a counter reference, micrometer-sized LTO powders (Bulk-LTO) were also examined. The XRD pattern and FESEM image of Bulk-LTO are displayed in the Supporting Information, Figure S1 and S2, respectively. The electrochemical performance of Bulk-LTO/Li and Meso-LTO-C/Li cells cycled between 1.0–2.5 V with two different electrode compositions 80:10:10 and 90:0:10, weight ratio, of LTO/C powders, CB (carbon black, conductive additive), and PVDF (poly(vinylidene fluoride), binder) are displayed in **Figure 5**. The cycling stability with variable rate is shown in Figure 5a for Bulk-LTO with Meso-LTO-C depicted in 5b. The charge capacity as a function of current density is plotted in Figures 5c and d, and reflects the second cycle capacity of each stage in Figures 5a and b, respectively. The Bulk-LTO with no CB (90:0:10, open hexagons in Figure 5c) exhibits only 61 mA h g^{-1} even at the low rate of 0.2 C, which is only 47% of the capacity at identical C-rate for the electrode with conductive additive and a composition of 80:10:10 (open triangles in Figure 5c). Furthermore, the Bulk-LTO with no CB has negligible capacity at 5 C. In sharp contrast, the Meso-LTO-C with no CB (closed rectangles in Figures 5b and d) exhibits almost the same capacity (141 mA h g^{-1}) as the Meso-LTO-C (144 mA h g^{-1}) with conductive additive (80:10:10, closed circle) at 0.2 C, and retains a very high capacity of 90 mA h g^{-1} at the significantly higher rate of 5 C. Collectively these results show the importance of electrical conductivity for the performance of LTO at high rate. More importantly, we have demonstrated that the porous carbon network of Meso-LTO-C acts as an excellent electrically conductive matrix and could replace excess conductive additive, thereby increasing the mass of the active material. Also by combining the Meso-LTO-C electrode with a small amount of CB (closed circle, 80:10:10) extraordinary rate performance is observed, 115 mA h g^{-1} at 10 C-rate with the Bulk-LTO combined with conductive additive (open triangles) exhibiting only 69 mA h g^{-1} at the same rate.

The charge–discharge voltage profiles of Bulk-LTO and Meso-LTO-C with 80:10:10 of active material:conductive additive:binder at different C-rates are displayed in **Figure 6**. There appears to be a larger capacity with sloping voltage profiles at 2.0–1.5 V and 1.5–1.0 V (vs. Li/Li^+) for Meso-LTO-C compared to Bulk-LTO. The contribution to this additional capacity in the sloping voltage regions is not due to carbon as we have confirmed that both the Meso-LTO-C and conductive additive explain only ~4 mA h g^{-1} of increased capacity. Rather, the capacities in the sloping voltage profiles may be associated with the solid solution domain, which is generally broadened for nanosized particles.[17,32] The significantly better performance

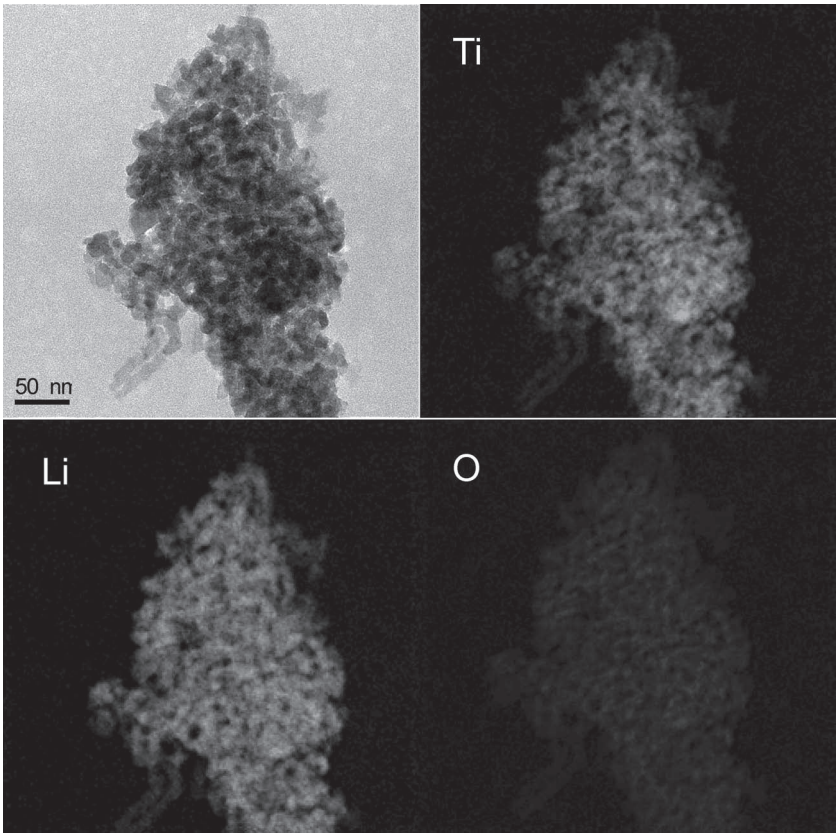

Figure 3. Electron energy-loss spectroscopy (EELS) mapping of Meso-LTO-C for the TEM image in the upper left corner showing wormhole-like pores.

of the Meso-LTO-C compared to that of the Bulk-LTO is attributed to the unique mesoporous carbon-composite nanostructure that allows for facile transport of both electrons and Li-ions. Most exceptionally, the Meso-LTO-C/Li cell also exhibits excellent *durability* at extremely high current, 10 C-rate, corresponding to only ~6 min for charge and discharge, as shown in **Figure 7**. Remarkably, after 500 cycles, 90% of the initial capacity is still retained, when cycled versus lithium metal. This implies that if LTO materials were employed in electric vehicles, employing our technology could enable the battery to be rapidly charged without significant degradation.

It is generally accepted that LTO is negligibly affected by surface side-reactions or the formation of an SEI film.[1b,3] However, to our knowledge there has not been an in-depth study on the effect of kinetics whether or not an SEI layer is formed on LTO. Thus the Meso-LTO-C/Li cell with an electrode composition of 80:10:10 was deeply discharged between 2.500–0.005 V for the first two cycles to intentionally form a SEI layer as depicted in Figures 5b and d. As observed for these two curves in Figure 5, the Meso-LTO-C with the SEI formed by pre-cycling with deep discharge down to 0.005 V (vs. Li/Li^+) (crossed circles) exhibits significantly poorer performance than that without deep discharge pre-cycling (closed circles). This is not a trivial result as it indicates SEI formation can detrimentally affect battery operation and that, for all materials, it is important to understand the formation and stability of the SEI layer.

To understand kinetic properties in depth depending on the nanostructure and the electrolyte-electrode interface as well as the SEI formation, AC impedance data for three different electrodes were compared: a) Bulk-LTO/Li, b) Meso-LTO-C/Li half-cells (HCs) after two cycles between 1.0–2.5 V (vs. Li/Li^+) with subsequent discharge to 60 mA g^{-1} at 0.2 C-rate as well as c) Meso-LTO-C/Li HC after two cycles between 0.005-2.500 V (vs. Li/Li^+) also with subsequent discharge to 60 mA g^{-1} at 0.2 C. The Nyquist plots of the three

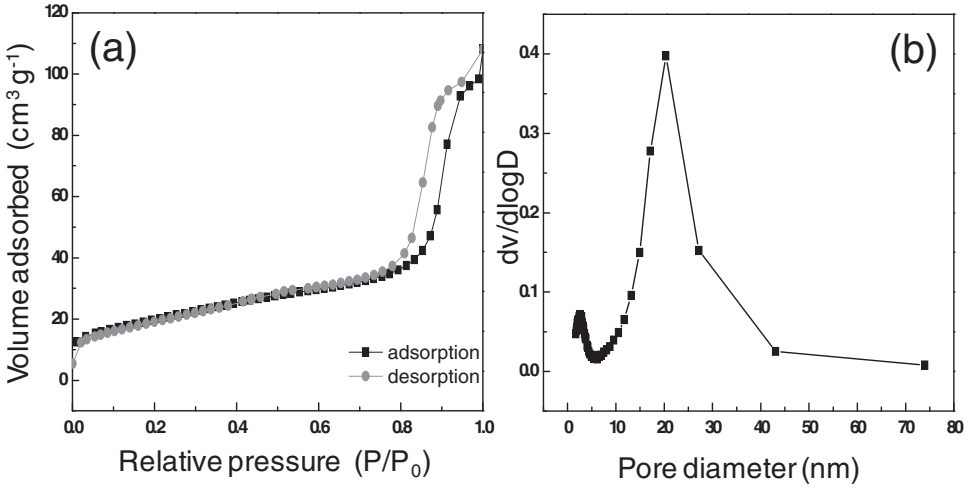

Figure 4. a) Nitrogen adsorption-desorption isotherms for Meso-LTO-C and b) the corresponding pore size distribution.

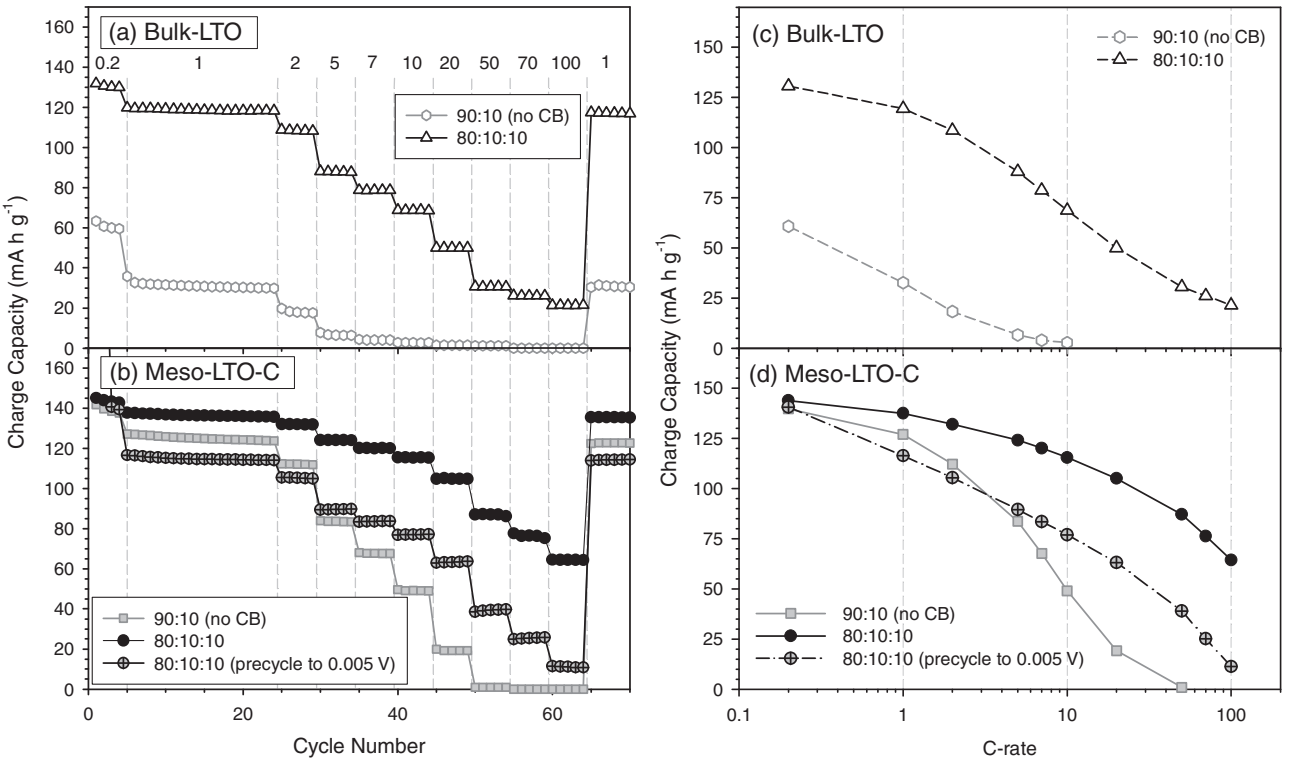

Figure 5. Cycling data with variable rate for (a) Bulk-LTO/Li and (b) Meso-LTO-C/Li cells cycled between 1.0-2.5 V (vs. Li/Li^+) as a function of electrode composition (active material:carbon black (CB):PVDF by weight) with the C-rate provided on the top axis. The charge capacity as a function of C-rate is plotted in (c) and (d) for Bulk-LTO/Li and Meso-LTO-C/Li, respectively. The rate performance of a Meso-LTO-C/Li cell after pre-cycling between 0.005-2.500 V (vs. Li/Li^+) at 0.2 C-rate for the first two cycles is also given for comparison to intentionally form a SEI layer in (b) and (d).

HCs are displayed in **Figures 8**a–c. To obtain a fair comparison, the resistance values are normalized by multiplying by the mass of the active material. The signals in Figures 8a–c show characteristic features comprised of semicircles (∗, #), followed by a constant slope at low frequency (*f*) (∧). The interpretation of the impedance signals is based on an equivalent circuit model comprised of resistance (*R*), capacitance (*C*), and Warburg term (*W*) related to the solid-state Li^+ diffusion into the bulk. Values for *R* and *C* connected in parallel may be fitted to the semicircle in the Nyquist plot (e.g., ∗ in Figure 8), and its radius corresponds to the *R* value while *W* accounts for the constant slope

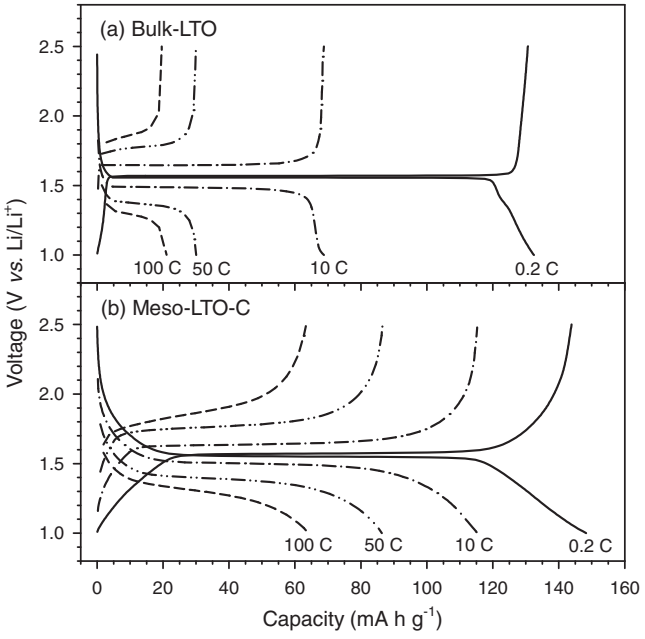

Figure 6. Charge–discharge voltage profiles of (a) Bulk-LTO/Li and (b) Meso-LTO-C/Li cells at different C-rates.

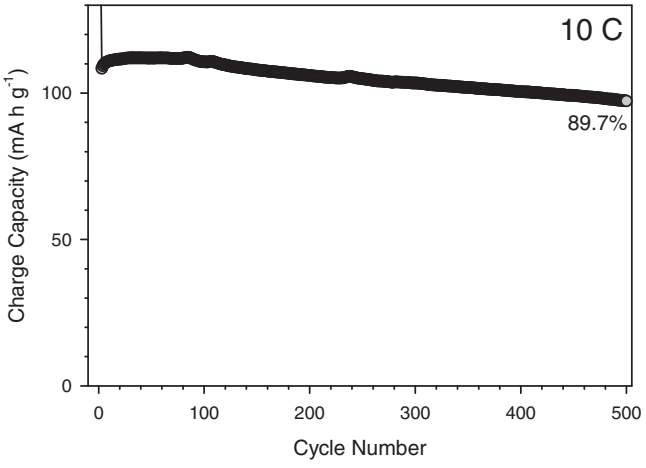

Figure 7. Cycling performance of the Meso-LTO-C/Li half cell at 10 C-rate between 1.0–2.5 V (vs. Li/Li^+). The first two cycles were at 0.2 C-rate.

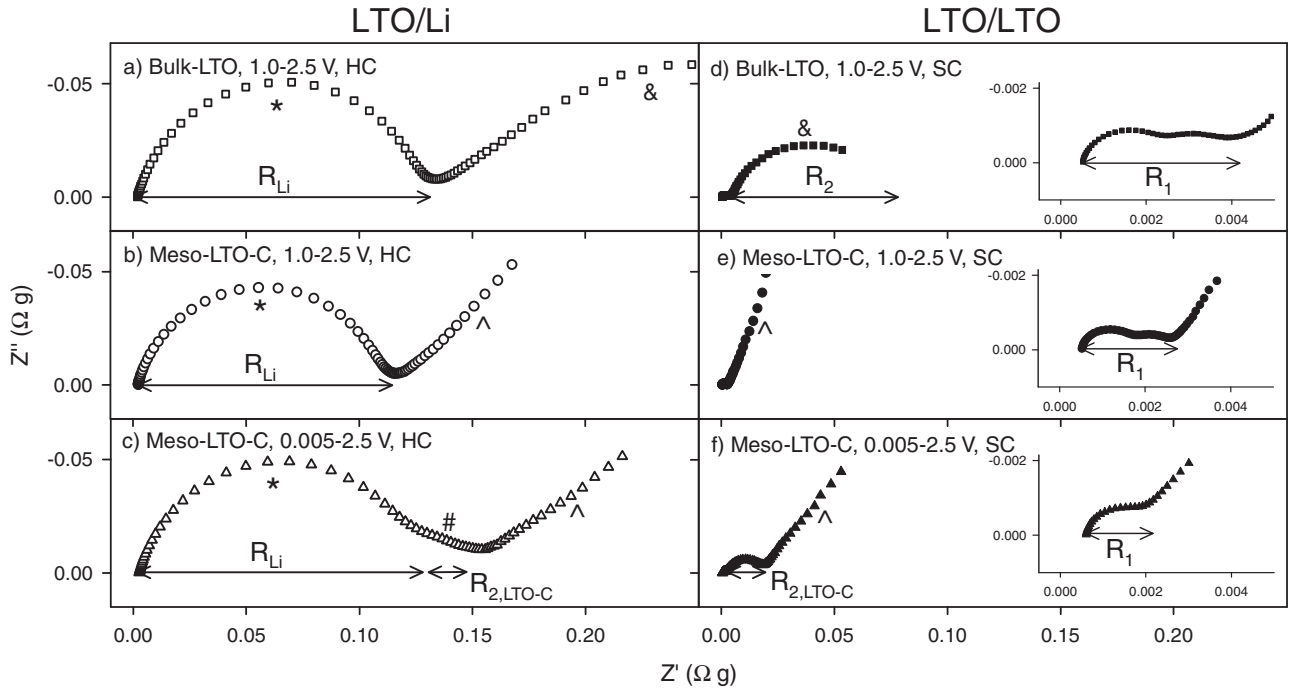

Figure 8. Nyquist plots of LTO/Li half cells (HCs) (a,b,c) and LTO/LTO symmetric cells (SCs) (d,e,f). a,d) Bulk-LTO, b,e) Meso-LTO-C after cycling between 1.0-2.5 V (vs. Li/Li^+) and subsequent discharge up to 60 mA h g^{-1} at 0.2 C-rate. c,f) Meso-LTO-C after cycling between 0.005–2.500 V (vs. Li/Li^+) and subsequent discharge up to 60 mA h g^{-1} at 0.2 C-rate. The *R* terms are explained in the main text and Figure 6. The scale is same in all plots. Enlarged views the high *f* region for (d,e,f) are provided in the insets.

region in the low *f* range (e.g., ∧ in Figure 8).[33] The equivalent circuit displayed in **Figure 9** is for the LTO/Li HC and is based on the well-known Voigt-type model.[34] R_0 is the resistance of the electrolyte solution, which is negligibly small in conventional laboratory cells, R_1 and R_2 may be related to the SEI and/or charge transfer resistance. Recently, some reports argue that the semicircle at high *f* may be more related to the electrical contact resistance rather than the resistance from the SEI;[35] C_3 accounts for finite diffusion length. R_{Li} is attributed to the SEI on the Li metal counter/reference electrode in HC even though this term is neglected in most previous reports.[14–16,36]

The impedance data using HCs in Figures 8a-c show semicircles at high *f* which have similar sizes. Considering that the LTO electrodes from the Bulk-LTO/Li and Meso-LTO/Li HC (Figures 8a and b) at normal cycling condition above 1 V (vs. Li/Li^+) will not have an SEI, the signals may come from electrical contact resistance, charge transfer resistance, SEI on Li metal, etc. Thus we have eliminated the signal from the SEI on Li metal by using a symmetric cell (SC) configuration where two identical LTO electrodes are used. The LTO electrode fashioned from HCs was cut in half, aligned oppositely, and divided by a single sheet of separator.[35] Figures 8d–f show the results of the LTO/LTO SCs. Surprisingly, the magnitude of the high *f* semicircles in the SCs in Figures 8d–f are not as intense as those for the HCs in Figures 8a–c, which indicates that these semicircles (*) are predominantly from the SEI on the Li metal, and not the LTO electrode. Also, the three different LTO/LTO SCs in Figures 8d–f exhibit quite different features. For Bulk-LTO SC (Figure 8d), very small semicircles at high *f* (R_1) and a subsequent large semicircle at medium-low *f* (R_2) are observed. For Meso-LTO-C SC (Figure 8e), even smaller semicircles (R_1) than that from Bulk-LTO are observed with only the Warburg-type diffusion term at medium-low *f* (∧). Considering that both Bulk-LTO and Meso-LTO-C at normal cycling conditions up to 1 V (vs. Li/Li^+) do not have an SEI, the small semicircles at high *f* (R_1) are most likely related to electrical contact resistance. The second large semicircle for Bulk-LTO (&, R_2) may be attributed to charge transfer resistance. The absence of this term in Meso-LTO-C in Figure 8e most likely explains the superior rate performance of Meso-LTO-C compared to Bulk-LTO. Furthermore, the Meso-LTO-C SC that was discharged to 0.005 V to allow SEI formation (Figure 8f), clearly shows a unique semicircle ($R_{2,LTO-C}$) at medium f compared to the Meso-LTO-C SC without an SEI (Figure 8e). This additional semicircle ($R_{2,LTO-C}$), not clearly observed separately in the Meso-LTO-C HC (#, Figure 8c), is attributed to the SEI layer formed during deep discharge to 0.005 V. The difference in

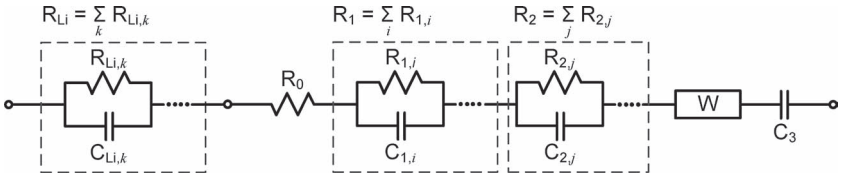

Figure 9. Equivalent circuit for LTO/Li half cell.

total R values for the Meso-LTO-C HC is not significant e.g.: without the SEI, discharge to 1 V, (mostly, R_{Li} in Figure 8b) and with SEI, discharge to 0.005 V (mostly, $R_{Li} + R_{2,LTO-C}$, Figure 8c). However, for the SCs, the total R value for the Meso-LTO-C discharged to 1 V (R_1 = ~3 mΩ g) is much smaller than that for the Meso-LTO-C discharged to 0.005 V to form an SEI ($R_1 + R_{2,LTO-C}$ = ≈21 mΩ g). This result clearly demonstrates that the SEI formed below 1 V (vs. Li/Li^+) will significantly contribute to the kinetics properties and that it is especially relevant to nanostructured systems.

3. Conclusions

A simple block copolymer assembly route was successfully employed to synthesize a mesostructured LTO-carbon composite with inorganic precursors. During heat-treatment at 700 °C employed for the crystallization of the amorphous metal oxide to form the spinel LTO structure, part of the polyisoprene was converted to a conductive carbon matrix that not only maintained the mesostructure but also provided electrical conductivity to the insulating LTO framework. Pore size was calculated to be 20.4 nm, large enough for facile diffusion of electrolyte to the LTO framework. The excellent rate capability of the mesostructured LTO-carbon composite, with 500 cycles demonstrated at 10 C and a capacity of ≈115 mA h g^{-1}, is attributed to the outstanding electrical conductivity of the mesoporous nanoarchitecture combined with the SEI-free surface as supported by the EIS analyses. This simple self-assembly method employing block copolymers with a sp^2-hybridized carbon-containing hydrophobic block can be extended to other active materials in order to enable improved rate performance for a variety of LIB electrodes.

4. Experimental Section

Synthesis of Mesoporous LTO: Poly(isoprene) -*b*-poly(ethylene oxide) block copolymer (PI-*b*-PEO) was synthesized by anionic polymerization. The M_n value and PEO fraction of PI-*b*-PEO used were found to be 30,000 g mol^{-1} and 0.06, respectively. PI-*b*-PEO has narrow weight distributions with a polydispersity index of 1.13. This PI-*b*-PEO block copolymer was used both as a structure directing agent as well as carbon source. Initially, 0.2 g of PI-*b*-PEO was dissolved in a mixture of 4 ml of THF. The inorganic precursor solution was prepared by mixing 1.287 ml of TTIP (titanium tetraisopropoxide) and 0.181g of lithium ethoxide (3.48 mL of 1 M $LiOC_2H_5$ in THF stock solution). 0.39 g of Oxalic acid was then added to the inorganic precursor solution. Block copolymer solution and inorganic precursor were mixed and stirred for 2 h. Films were cast by evaporation of the solvents on a hot plate at 50 °C, and further dried at 130 °C in a vacuum oven for 1 h. The as-synthesized films were heat-treated to 700 °C under N_2 and held for 2 h. To prepare bulk the LTO sample, a typical solid-state method was employed using a stoichiometric amount of TiO_2 (anatase) and Li_2CO_3. The mixture powder was heat-treated at 800 °C for 20 h under atmosphere. (Supporting Information, Figure S2: XRD pattern of bulk LTO, Figure S3: SEM of bulk LTO)

Characterization: TEM and HRTEM characterizations were carried out using an EM-2010 microscope (JEOL Ltd.). The XRD study was performed with an X'Pert diffractometer (Cu Kα radiation; PANalytical) with an X'Celerator detector (PANalytical). Nitrogen adsorption experiments were carried out using Micromeritics Tristar II 3020 system (Micromeritics Instrument Corporation). SAXS data were collected with an apparatus consisting of an 18-kW rotating anode X-ray generator (Cu Kα wavelength = 1.542 Å, Rigaku Co.) and a one-dimensional position-sensitive detector (M. Braun Co.).

Electrochemical Characterization: The mesoporous LTO/C composite electrodes were prepared by spreading LTO/C powders, CB (super C65, TIMCAL Ltd.), and PVDF on a piece of Cu foil. 2032-type coin cells with two-electrodes (Mesoporous LTO/C)/Li were assembled in an Ar-filled dry box. 1.0 M $LiPF_6$ in a mixture of ethylene carbonate (EC) and diethyl carbonate (DEC) (1:1 volume ratio) was used as the electrolyte. Porous 25 μm thick polypropylene (PP)/polyethylene/PP trilayer film (2325, Celgard) were used as separators. Unless specifically specified, galvanostatic charge-discharge cycling was performed between 1.0–2.5 V (vs. Li/Li^+) at different C-rates at room temperature. In this report, lithiation was expressed as discharging and de-lithiation as charging because Li foil was used as the counter electrode in the HCs. The electrochemical impedance spectroscopy (EIS) study was performed using a 1280C Solartron instrument. The AC impedance measurements were recorded using a signal with an amplitude of 5 mV and a frequency range from 500 kHz to 5 mHz. The first measurement was performed using the LTO/Li half cells after pre-cycling between 1.0–2.5 V (vs. Li/Li^+) or 0.005–2.500 V (vs. Li/Li^+), and subsequently discharging up to 60 mA h g^{-1}. After the measured LTO/Li HCs were disassembled, the collected LTO electrodes were reassembled as LTO/LTO SCs inside the glove box. Then, the second measurement was performed using the LTO/LTO SCs. The composition of the electrodes used for the EIS measurements was 80:10:10 (LTO:CB:PVDF weight ratio). The specific capacity is based on the total weight of LTO and carbon. In this report, lithiation is expressed as discharging and delithiation as charging because Li foil is used as the counter electrode in the HCs.

Supporting Information

Supporting Information is available from the Wiley Online Library or from the author.

Acknowledgements

E.K. and Y.S.J. contributed equally to this work. This work was supported by the Mid-career Researcher Program (2009-0084771) through an NRF grant funded by the MEST and by the second stage of the BK 21 program of Korea. This research was further supported by the National Creative Research Initiative Program supported by the National Research Foundation of Korea (NRF). This research was also supported by the U.S. Department of Energy under Contract No. DE-AC36-08-GO28308 through: the NREL Laboratory Directed Research and Development Program with the National Renewable Energy Laboratory. U.W. gratefully acknowledges financial support of the National Science Foundation (award DMR-0605856).

Received: May 9, 2011
Revised: July 5, 2011
Published online: September 9, 2011

[1] a) J. M. Tarascon, M. Armand, *Nature* **2001**, *414*, 359; b) A. S. Arico, P. Bruce, B. Scrosati, J. M. Tarascon, W. Van Schalkwijk, *Nat. Mater.* **2005**, *4*, 366; c) K. Kang, Y. S. Meng, J. Breger, C. P. Grey, G. Ceder, *Science* **2006**, *311*, 977; d) M. Armand, J. M. Tarascon, *Nature* **2008**, *451*, 652; e) X. Ji, K. T. Lee, L. F. Nazar, *Nat. Mater.* **2009**, *8*, 500; f) J. M. Tarascon, *Phil. Trans. R. Soc. A* **2010**, *368*, 3227; g) C. Ban, Z. Wu, D. T. Gillaspie, L. Chen, Y. Yan, J. L. Blackburn, A. C. Dillon, *Adv. Mater.* **2010**, *22*, E145.

[2] a) K. M. Colbow, J. R. Dahn, R. R. Haering, *J. Power Sources* **1989**, *26*, 397; b) E. Ferg, R. J Gummow, A. De Kock, M. M. Thackeray,

J. Electrochem. Soc. **1994**, *141*, L147; c) T. Ohzuku, A. Ueda, N. Yamamoto, *J. Electrochem. Soc.* **1995**, *142*, 1431; d) Z. Yang, D. Choi, S. Kerisit, K. M. Rosso, D. Wang, J. Zhang, G. Graff, J. Liu, *J. Power Sources* **2009**, *192*, 588; e) W. J. H. Borghols, M. Wagemaker, U. Lafont, E. M. Kelder, F. M. Mulder, *J. Am. Chem. Soc.* **2009**, *131*, 17786.

[3] a) S. Huang, Z. Wen, J. Zhang, Z. Gu, X. Xu, *Solid State Ionics* **2006**, *177*, 851; b) E. M. Sorensen, S. J. Barry, H. K. Jung, J. M. Rondinelli, J. T. Vaughey, K. R. Poeppelmeier, *Chem. Mater.* **2006**, *18*, 482.

[4] a) E. Peled, *J. Electrochem. Soc.* **1979**, *126*, 2047; b) R. Fong, U. von Sacken, J. R. Dahn, *J. Electrochem. Soc.* **1990**, *137*, 2009; c) D. Aurbach, Y. Ein Eli, O. Chusid, Y. Carmeli, M. Babai, H. Yamin, *J. Electrochem. Soc.* **1994**, *141*, 603; d) E. Peled, D. Golodnitsky, G. Ardel, *J. Electrochem. Soc.* **1997**, *144*, L208; e) R. Imhof, P. Novak, *J. Electrochem. Soc.* **1998**, *145*, 1081; f) H. L. Zhang, F. Li, C. Liu, J. Tan, H. M. Cheng, *J. Phys. Chem. B* **2005**, *109*, 22205; g) M. E. Spahr, H. Buqa, A. Wursig, D. Goers, L. Hardwick, P. Novak, F. Krumeich, J. Dentzer, C. Vix-Guterl, *J. Power Sources* **2006**, *153*, 300; h) Y. S. Jung, A. S. Cavanagh, L. A. Riley, S. H. Kang, A. C. Dillon, M. D. Groner, S. M. George, S. H. Lee, *Adv. Mater.* **2010**, *22*, 2172.

[5] a) K. C. Moller, T. Hodal, W. K. Appel, M. Winter, J. O. Besenhard, *J. Power Sources* **2001**, *97*, 595; b) H. Yang, H. Bang, K. Amine, J. Prakash, *J. Electrochem. Soc.* **2005**, *152*, A73; c) T. Doi, L. Zhao, M. Zhou, S. Okada, J. Yamaki, *J. Power Sources* **2008**, *185*, 1380; d) J. Mun, Y. S. Jung, T. Yim, H. Y. Lee, H. J. Kim, Y. G. Kim, S. M. Oh, *J. Power Sources* **2009**, *194*, 1068; e) I. D. Scott, Y. S. Jung, A. S. Cavanagh, Y. Yan, A. C. Dillon, S. M. George, S.-H. Lee, *Nano Lett.* **2011**, *11*, 414.

[6] a) C. K. Chan, H. Peng, G. Liu, K. McIlwrath, X. F. Zhang, R. A. Huggins, Y. Cui, *Nat. Nanotech.* **2008**, *3*, 31; b) H. Kim, J. Cho, *Nano Lett.* **2008**, *8*, 3688; c) M. H. Park, M. G. Kim, J. Joo, K. Kim, J. Kim, S. Ahn, Y. Cui, J. Cho, *Nano Lett.* **2009**, *9*, 3844; d) J. Cabana, L. Monconduit, D. Larcher, M. R. Palacin, *Adv. Mater.* **2010**, *22*, E170.

[7] X. W. Zhang, Y. Li, S. A. Khan, P. S. Fedkiw, *J. Electrochem. Soc.* **2004**, *151*, A1257.

[8] a) S. Tobishima, J. Yamaki, *J. Power Sources* **1999**, *81*, 882; b) P. G. Balakrishnan, R. Ramesh, T. Prem Kumar, *J. Power Sources* **2006**, *155*, 401.

[9] K. Ariyoshi, R. Yamato, T. Ohzuku, *Electrochim. Acta* **2005**, *51*, 1125.

[10] Y. Koyama, T. E. Chin, U. Rhyner, R. K. Holman, S. R. Hall, Y. M. Chiang, Adv. *Funct. Mater.* **2006**, *16*, 492.

[11] a) S. Takai, M. Kamata, S. Fujine, K. Yoneda, K. Kanda, T. Esaka, *Solid State Ionics* **1999**, *123*, 165; b) K. Zaghib, M. Simoneau, M. Armand, M. Gauthier, *J. Power Sources* **1999**, *81*, 300.

[12] C. H. Chen, J. T. Vaughey, A. N. Jansen, D. W. Dees, A. J. Kahaian, T. Goacher, M. M. Thackeray, *J. Electrochem. Soc.* **2001**, *148*, A102.

[13] L. Cheng, J. Yan, G. N. Zhu, J. Y. Luo, C. X. Wang, Y. Y. Xia, *J. Mater. Chem.* **2010**, *20*, 595.

[14] L. Shen, C. Yuan, H. Luo, X. Zhang, K. Xu, F. Zhang, *J. Mater. Chem.* **2011**, *21*, 761.

[15] S. Huang, Z. Wen, X. Zhu, Z. Gu, *Electrochem. Commun.* **2004**, *6*, 1093.

[16] B. Zhang, H. Du, B. Li, F. Kang, *Electrochem. Solid-State Lett.* **2010**, *13*, A36.

[17] K. S. Park, A. Benayad, D. J. Kang, S. G. Doo, *J. Am. Chem. Soc.* **2008**, *130*, 14930.

[18] a) S. H. Lee, Y. H. Kim, R. Deshpande, P. A. Parilla, E. Whitney, D. T. Gillaspie, K. M. Jones, A. H. Mahan, S. Zhang, A. C. Dillon, *Adv. Mater.* **2008**, *20*, 3627; b) Y. Ren, A. R. Armstrong, F. Jiao, P. G. Bruce, *J. Am. Chem. Soc.* **2010**, *132*, 996.

[19] K. Amine, I. Belharouak, Z. Chen, T. Tran, H. Yumoto, N. Ota, S. T. Myung, Y. K. Sun, *Adv. Mater.* **2010**, *22*, 3052.

[20] a) J. S. Beck, J. C. Vartuli, W. J. Roth, M. E. Leonowicz, C. T. Kresge, K. D. Schmitt, C. T. W. Chu, D. H. Olson, E. W. Sheppard, S. B. McCullen, J. B. Higgins, J. L. Schlenker, *J. Am. Chem. Soc.* **1992**, *114*, 10834; b) P. T. Tanev, M. Chibwe, T. J. Pinnavaia, *Nature* **1994**, *368*, 321; c) S. A. Bagshaw, E. Prouzet, T. J. Pinnavaia, *Science* **1995**, *269*, 1242; d) D. Zhao, J. Feng, Q. Huo, N. Melosh, G. H. Fredrickson, B. F. Chmelka, G. D. Stucky, *Science* **1998**, *279*, 548; e) Z. Zhang, T. J. Pinnavaia, *J. Am. Chem. Soc.* **2002**, *124*, 12294.

[21] Y. Shi, B. Guo, S. A. Corr, Q. Shi, Y. S. Hu, K. R. Heier, L. Chen, R. Seshadri, G. D. Stucky, *Nano Lett.* **2009**, *9*, 4215.

[22] a) F. Jiao, K. M. Shaju, P. G. Bruce, *Angew. Chem. Int. Ed.* **2005**, *44*, 6550; b) F. Jiao, J. Bao, A. H. Hill, P. G. Bruce, *Angew. Chem. Int. Ed.* **2008**, *47*, 9711; c) Y. Ren, L. J. Hardwick, P. G. Bruce, *Angew. Chem. Int. Ed.* **2010**, *49*, 2570.

[23] a) D. M. Antonelli, J. Y. Ying, *Angew. Chem. Int. Ed.* **1996**, *35*, 426; b) P. Yang, D. Zhao, D. I. Margolese, B. F. Chmelka, G. D. Stucky, *Nature* **1998**, *396*, 152.

[24] a) S. Scharner, W. Weppner, P. Schmid-Beurmann, *J. Electrochem. Soc.* **1999**, *146*, 857; b) H. Ge, N. Li, D. Li, C. Dai, D. Wang, *Electrochem. Commun.* **2008**, *10*, 719; c) J. Shu, *J. Solid State Electrochem.* **2009**, *13*, 1535.

[25] J. Lee, M. C. Orilall, S. C. Warren, M. Kamperman, F. J. DiSalvo, U. Wiesner, *Nat. Mater.* **2008**, *7*, 222.

[26] a) J. Lee, S. Yoon, S. M. Oh, C. H. Shin, T. Hyeon, *Adv. Mater.* **2000**, *12*, 359; b) P. T. Tanev, T. J. Pinnavaia, *Science* **1995**, *267*, 865.

[27] A. C. Dillon, M. Yudasaka, M. S. Dresselhaus, *J. Nanosci. Nanotechnol.* **2004**, *4*, 691.

[28] A. D. Krawitz, *Introduction to Diffraction in Materials Science and Engineering.*Wiley: New York, **2001**; p 168.

[29] R. Ryoo, J. M. Kim, C. H. Ko, C. H. Shin, *J. Phys. Chem.* **1996**, *100*, 17718.

[30] M. Kruk, M. Jaroniec, *Chem. Mater.* **2001**, *13*, 3169.

[31] W. Dong, Y. Sun, C. W. Lee, W. Hua, X. Lu, Y. Shi, S. Zhang, J. Chen, D. Zhao, *J. Am. Chem. Soc.* **2007**, *129*, 13894.

[32] a) G. Sudant, E. Baudrin, D. Larcher, J.-M. Tarascon, *J. Mater. Chem.* **2005**, *15*, 1263; b) M. Wagemaker, D. R. Simon, E. M. Kelder, J. Schoonman, C. Ringpfeil, U. Haake, D. Lützenkirchen-Hecht, R. Frahm, F. M. Mulder, *Adv. Mater.* **2006**, *18*, 3169; c) M. Wagemaker, W. J. H. Borghols, F. M. Mulder, *J. Am. Chem. Soc.* **2007**, *129*, 4323.

[33] A. J. Bard, L. R. Faulkner, *Electrochemical Methods: Fundamentals and Applications.*John Wiley & Sons, New York, **2001**, Ch. 10.

[34] a) A. Zaban, E. Zinigrad, D Aurbach, *J. Phys. Chem.* **1996**, *100*, 3089; b) D. Aurbach, M. D. Levi, E. Levi, H. Teller, B. Markovsky, G. Salitra, U. Heider, L. Heider, *J. Electrochem. Soc.* **1998**, *145*, 3024.

[35] a) M. Gaberscek, J. Moskon, B. Erjavec, R. Dominko, J. Jamnik, Electrochem.*Solid-State Lett.* **2008**, *11*, A170; b) J.-M. Atebamba, J. Moskon, S. Pejovnik, M. Gaberscek, *J. Electrochem. Soc.* **2010**, *157*, A1218.

[36] a) L. Cheng, X. L. Li, H. J. Liu, H. M. Xiong, P. W. Zhang, Y. Y. Xia, *J. Electrochem. Soc.* **2007**, *154*, A692; b) K. C. Hsiao, S. C. Liao, J. M. Chen, *Electrochim. Acta* **2008**, *53*, 7242.